An Experimental Study of Melting of Binary Mixtures with Double-Diffusive Convection in the Liquid

C. Beckermann
Department of Mechanical Engineering, The University of Iowa, Iowa City, Iowa

R. Viskanta
Heat Transfer Laboratory, School of Mechanical Engineering, Purdue University, West Lafayette, Indiana

■An experimental study is reported of the melting of a vertical ice layer into an ammonium chloride–water solution, as well as the melting of a vertical ammonium chloride–water eutectic layer into water. The experiments were conducted inside a vertical rectangular cavity with differentially heated side walls. It is found that in both cases the melting process induces the formation of double-diffusive layers in the initially homogeneous liquid. Due to the continuously changing concentrations in each layer, the double-diffusive interfaces can break up, resulting in vigorous mixing of the liquid in the layers. These convection phenomena have a significant influence on the local melting rates. It is observed that the presence of the double-diffusive interfaces in the liquid causes the formation of steps in the solid layer thickness, while the changing height of the double-diffusive layers can even induce resolidification on parts of the remaining solid layer.

Keywords: *melting and solidification processes, solid–liquid phase change, double-diffusion systems, binary systems*

INTRODUCTION

Solid–liquid phase change in binary systems has recently received increased research attention due to its large variety of applications, including solidification of castings [1], crystal growth [2], magmatic crystallization and melting [3], and melting of ice in oceans [4]. It is now well recognized that natural convection in the liquid has a profound influence on the melting and solidification processes [1–4]. During the phase change of substances consisting of more than a single chemical species, natural convection is caused by the simultaneous action of thermal and solutal driving forces. Because most fluids have vastly different molecular diffusivities for heat and species, such natural convention is often called double-diffusive convection [5].

Double-diffusive convection during phase change in binary systems has been the subject of a number of recent investigations [1–7]. During both melting and solidification in containers, complex convection patterns have been observed. Even in an initially homogeneous liquid, double-diffusive convection can be induced by the phase-change process itself [3]. Huppert and Turner [4] have reported an experimental study of the melting of a vertical ice surface into a salinity gradient inside an enclosure. Because of its lower salinity, the melt water is less dense than the surroundings and rises along the ice surface in a thin concentration boundary layer toward the top of the enclosure. Eventually, the melt water is mixed outwards into a series of horizontal layers of different compositions separated by relatively thin (double-diffusive) interfaces. The melting rates are substantially influenced by the different environments created by these layers.

Of related interest are experimental studies considering boundary layer flow during free convection melting of ice in saline water [8–11]. Depending on the temperature and salinity of the ambient water, a number of distinctively different flow regimes have been observed. Typically, a relatively thin, upward-flowing concentration boundary layer is established near the ice surface. The thermal boundary layer is, however, considerably thicker, and the flow field can be upward or downward, depending on the magnitude and direction of the net buoyancy force at any location. The local melting rates can increase significantly in regions where the outer flow changes its direction, resulting in complex shapes of the ice surface at later times.

A review of the literature shows that melting of binary systems inside enclosures has received little research attention. Most of the earlier studies are qualitative in nature and limited to the melting of ice into saline solutions. It is the purpose of this paper to report on a series of experiments on the melting of a vertical layer of pure ice into a binary aqueous solution, as well as the melting of a binary solid into pure water. The experiments were performed inside a rectangular cavity with two vertical side walls maintained at uniform temperatures and the connecting walls well insulated (see Fig. 1). Shadowgraph and flow visualization, as well as temperature and species concentration measurements, were conducted to study the double-diffusive convection phenomena induced by the melting process. Corresponding analyses and numerical simulation of one of the present experiments are reported elsewhere [6, 7]. The interested reader is referred to other studies considering solidification in binary systems with double-diffusive convection in the melt [12, 13].
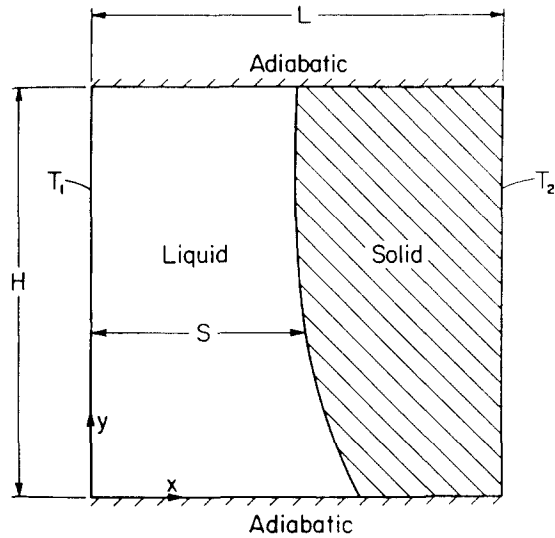
Figure 1. Schematic of the experimental configuration and coordinate system.

EXPERIMENTS

Test Cell and Instrumentation

Experiments were performed in a well-insulated test cell of square cross section. The test cell had inside dimensions of 4.76 cm in height and width and 3.81 cm in depth. The horizontal bottom wall was constructed of a phenolic plate, while the top wall and the vertical front and back walls were made of 6.4 mm thick Lexan. The two vertical sidewalls, which served as the heat source/sink, were multipass heat exchangers machined out of copper plate. The heat exchangers were connected through a valve system to two constant-temperature baths (Haake A82). Each heat exchanger contained three loops through which the flow rate could be controlled independently. The temperatures of each heat exchanger were measured with three thermocouples epoxied separately into small-diameter holes that were drilled close to the surface of the copper plate facing the fluid. In all experiments, the temperatures of each heat exchanger were uniform to within 0.1 °C of the desired temperature. The entire test cell was insulated with 2.53 cm thick Styrofoam.

Measurement of the temperature distribution inside the test cell was made with 33 thermocouples with a wire diameter of 0.127 mm. They were placed in three different rakes, which were located at heights of 0.635, 2.38, and 4.125 cm measured from the bottom of the test cell. The rakes were positioned such that the temperatures were measured along the vertical centerplane of the test cell. The rakes were oriented perpendicular to the flow direction to minimize their influence on the flow. The uncertainty in the location of each thermocouple bead was approximately ±0.2 mm. All thermocouples were calibrated with an accuracy of ±0.1°C. The thermocouples were connected to a HP-85 data logger and computer through which the temperatures could be measured and stored at preselected time intervals.

Qualitative observations of the density distribution and the flow structure in the liquid region were made using a shadowgraph system. The light source consisted of a collimated beam from a mercury arc lamp. After passing through the test cell, the light was imaged on a white glass plate and photographed using a high-sensitivity film (Kodak Tmax 400). Flow visualization was also performed by injecting a Calcoid Blue ink solution in the liquid region. In the flow-visualization experiments, the test cell was illuminated from the back through the Lexan windows using a white light source and a diffusing white glass plate. The ink solution was allowed to convect with the flow for some time, and the entire test cell was then photographed from the front. In both the shadowgraph and the flow-visualization experiments the solid region was masked with black paper; this was done to avoid reflections and scattering of the light by the solid and to increase the contrast between the liquid and solid regions (since ice is transparent). While the photographs were being taken, the insulation covering the liquid region was removed.

Concentration measurements were performed by withdrawing a few drops of the liquid with a hypodermic needle at the desired location in the test cell and analyzing them with a refractometer (Kernco). The refractometer was calibrated for the aqueous solution used in the present experiments (ie, NH_4Cl-H_2O) with an accuracy of ±0.2 wt % (NH_4Cl). In all experiments, the concentration measurements were made at several heights in the vertical center plane of the test cell, midway between the left wall and the solid-liquid interface. The uncertainty in the location of the tip of the hypodermic needle was approximately 1.0 mm.

Finally, it should be mentioned that the various measurements (see above) were conducted in separate tests so that they did not interfere with each other.

Test Materials and Conditions

In all experiments, solutions of ammonium chloride (NH_4Cl) in once-distilled, degasified water (H_2O) were used as the binary phase-change material. The equilibrium phase diagram of the NH_4Cl-H_2O system (see Fig. 2) is of the eutectic type with a eutectic temperature T_E of 257.75 K and concentration C_E of 0.197 wt fraction NH_4Cl, respectively [14]. All mixtures used in the present experiments were on the water-rich side of the eutectic point, so that the concentrations are conveniently expressed in terms of the weight fractions NH_4Cl (ie, $0 < C < 0.197$). On the water-rich side of the eutectic point, the liquidus line has a slope of approximately $\Gamma = -78.2$ K (with $T_p = 273.15$ K) and the segregation coefficient κ is equal to zero [14]. In presenting the experimental results, the temperatures and concentrations were nondimensionalized utilizing the eutectic temperature T_E and concentration C_E as well as the left wall temperature T_1 as reference values (see Nomenclature).

A number of experiments with different initial and boundary conditions were conducted [6]. For conciseness, only three experiments are reported here. The conditions for these experiments are summarized in Table 1. In experiments M1 and M2, the initial concentration of the liquid was equal to the eutectic concentration (ie, $C_1 = C_E = 0.197$), while the solid consisted of pure ice (ie, $C_2 = 0$). The opposite case was chosen for experiment M3, where the initial liquid (C_1) and solid (C_2) concentrations were equal to 0 and 0.197, respectively. Experiments M1 and M2 differ from each other in that the vertical side walls were held at different temperatures (see Table 1). With the present boundary and initial conditions, no density maximum of the NH_4Cl-H_2O solution was encountered during the experiments [14]. It is believed that the present set of experiments is representative of a larger variety of initial
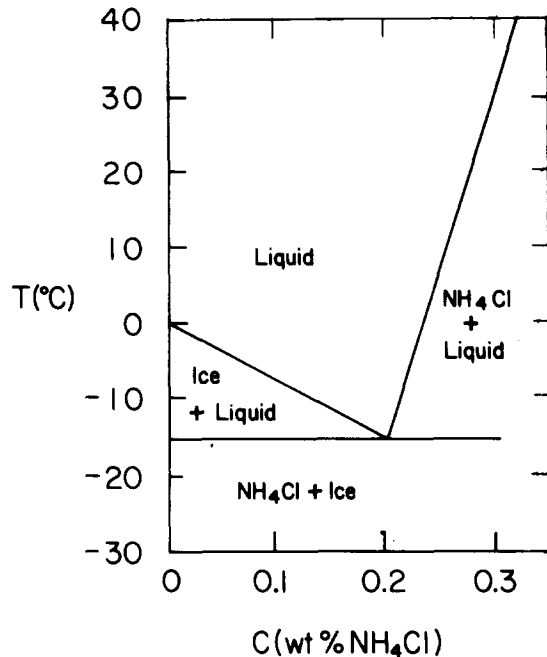
Figure 2. Equilibrium phase diagram of the NH$_4$Cl-H$_2$O system.

concentrations and thermal boundary conditions because of the simple nature of the NH$_4$Cl-H$_2$O phase diagram (see Fig. 2). This was also confirmed by performing experiments with other initial and boundary conditions, and the results were found to correspond closely to those of the experiments reported here [6].

Experimental Procedures

In preparing for the experiments, the entire test cell was first filled with liquid of concentration C_2. By lowering the right heat exchanger below the liquidus temperature, a vertical solid layer was formed at that wall. During the solidification process, the liquid was continuously stirred to prevent the formation of small air pockets in the solid, as well as to ensure a vertical and flat solid-liquid interface. When the desired thickness of the solid layer was reached (ie, $L - S_{in}$), the remaining liquid was quickly siphoned out of the test cell. Then the two heat exchangers were brought to the temperatures desired as the boundary (and initial) conditions (ie, T_1 and T_2). After the solid layer reached a uniform temperature, equal to T_2, the liquid of the desired initial concentration C_1 and temperature T_1 was carefully siphoned into the test cell. At this time, the experiment started.

It should be mentioned that the temperatures and concentrations started changing during the filling period. Temperature measurements as well as visual observations indicated, how-

Table 1. Summary of the Test Conditions for the Melting Experiments

Experiment	T_1 (°C)	T_2 (°C)	C_1	C_2	S_{in}
M1	0	0	0.197	0	0.5
M2	40	−20	0.197	0	0.5
M3	30	−20	0	0.197	0.4

ever, that the filling process did not have a major influence on the experiments at later times. This was also confirmed by repeating the same experiment several times using different filling procedures. Almost no differences in the temperatures and flow patterns were observed approximately 1 min after the filling process was completed.

Throughout all experiments it was observed that the solid layer thickness was relatively uniform over the depth of the test cell, indicating that three-dimensional heat and fluid flow effects were relatively weak. Furthermore, it was found that the convection processes and melting rates in the tests with the thermocouple rakes present did not significantly differ from the tests without the rakes.

RESULTS AND DISCUSSION

Melting of Ice into an Ammonium Chloride Solution

Experiment M1. The results for experiment M1 are shown in Figs. 4-6. When the ice melts into the NH$_4$Cl-H$_2$O solution, the liquid adjacent to the solid-liquid interface becomes rich in water. This compositional change causes the density to decrease, and the liquid confined in a thin concentration boundary layer rises along the interface. Reaching the top of the enclosure, the water-rich liquid spreads horizontally and forms a layer above the fluid of the original composition (see Fig. 3a). The concentration measurements (Fig. 6) as well as the flow visualization (Figs. 4b and 5b) indicate that this top layer is stably stratified, with the concentration (and density) decreasing toward the top. On the other hand, the liquid below the top layer is completely uncontaminated by the melt water and is compositionally homogeneous (Fig. 6). Because the dye had the same composition as the initial concentration of the liquid (ie, Φ_1), most of it is confined to the uncontaminated bottom later and does not mix with the diluted liquid. Only a small amount of dye is carried through the concentration boundary layer into the stratified region, where it slowly spreads out. Most of the fluid does not reach the top of the enclosure but spreads horizontally at a height in the top layer where its density is equal to the surrounding density (see also Figs. 4b and 5b). This indicates that the composition of the fluid in the concentration boundary layer is not uniform. The fluid closest to the interface has the highest water content and therefore rises to the top of the enclosure, while the fluid from the outer regions of the concentration boundary layer is less diluted and reaches its equilibrium height at a lower level. Similar convection phenomena have been observed in other experiments [3, 4].

Since the ice and the liquid at the interface are in local equilibrium, the compositional change also causes the temperatures of the interface to decrease, according to the equilibrium phase diagram, Fig. 2. The temperature profiles (Figs. 3b, 4c, and 5c) show sharp discontinuities at the solid-liquid interface, due to the latent heat absorption during melting. With the interfacial temperatures being below the right wall temperature (ie, 0°C), heat is conducted through the solid ice toward the interface. On the liquid side, the interfacial temperature depression results in an increase in the density of the fluid adjacent to the interface. Inside the concentration boundary layer, the density decrease due to the compositional change exceeds the density increase due to the lower temperature, so that the flow is upwards. Similarly, the isotherms in the top layer are relatively straight (see Figs. 3b, 4c, and 5c),

(a)

(b)
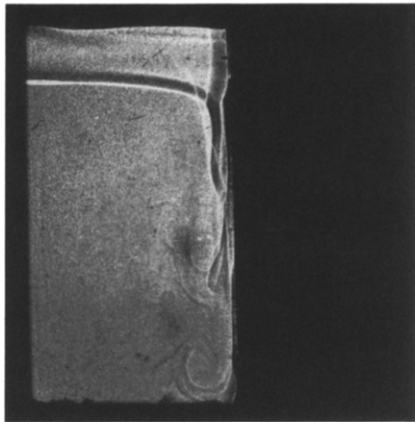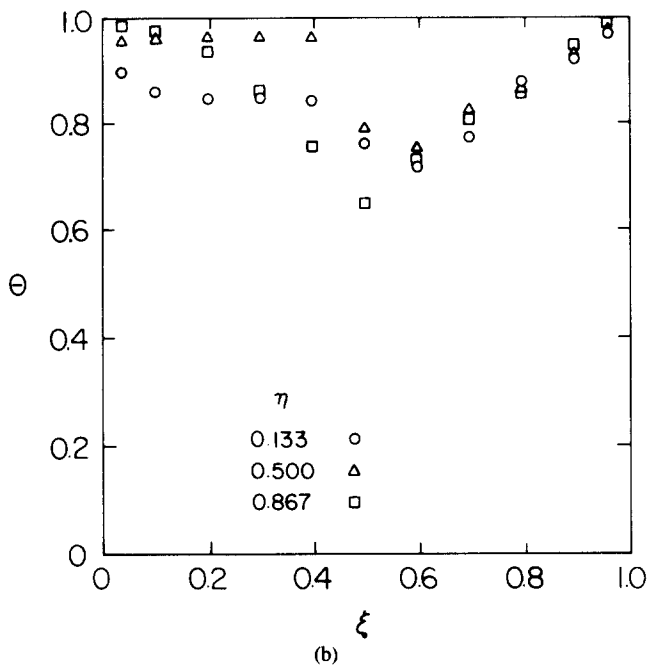
Figure 3. Results of experiment M1 at $t = 2$ min. (a) Shadowgraph; (b) temperature profiles.

indicating that the thermal buoyancy forces are not able to offset the stable concentration stratification and that heat transfer is mostly by conduction. In the uncontaminated fluid of the original composition, however, the interfacial temperature decrease causes thermal natural convection to develop. In the region outside the concentration boundary layer, the liquid flows downwards in a thermal boundary layer. The thermal boundary layer is much thicker than the concentration boundary layer, because of the large value of the Lewis number. Since the left wall is above the interface temperature, the liquid flows upwards at this wall and a clockwise rotating convection cell is established in the uncontaminated fluid (see Figs. 4b and 5b). Accordingly, the temperature profiles in the convecting bottom layer show sharp gradients at the left wall and the solid–liquid interface, while the core region is characterized by almost horizontal profiles (see Figs. 3b, 4c, and 5c). Note that all of these heat convection and conduction processes are due solely to the melting temperature depression caused by the

(a)

(b)

(c)
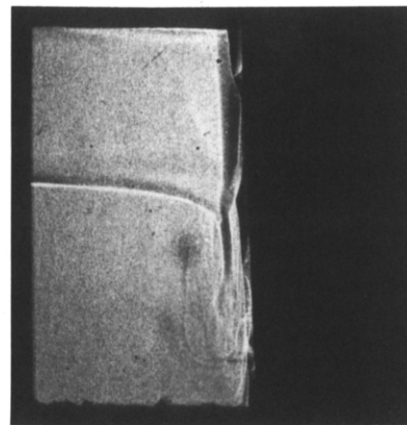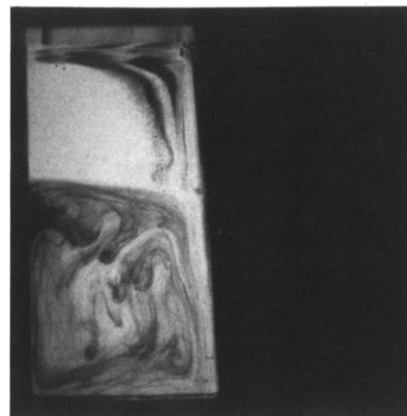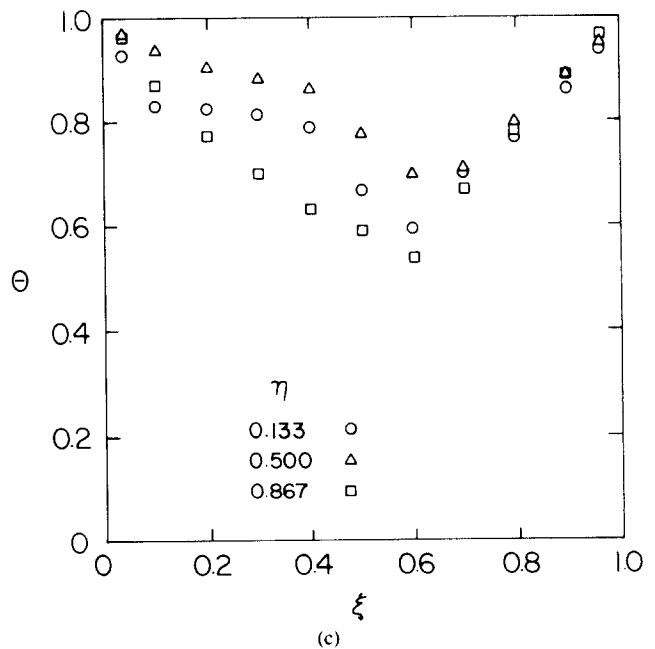
Figure 4. Results of experiment M1 at $t = 10$ min. (a) Shadowgraph; (b) flow visualization; (c) temperature profiles.

(a)

(b)

(c)
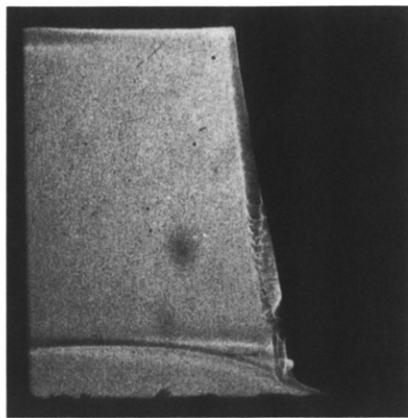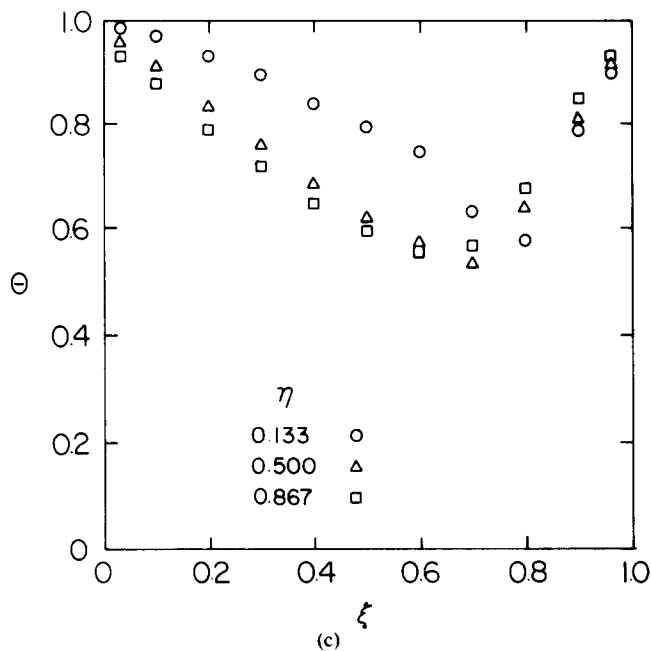
Figure 5. Results of experiment M1 at t = 30 min. (a) Shadowgraph; (b) flow visualization; (c) temperature profiles.
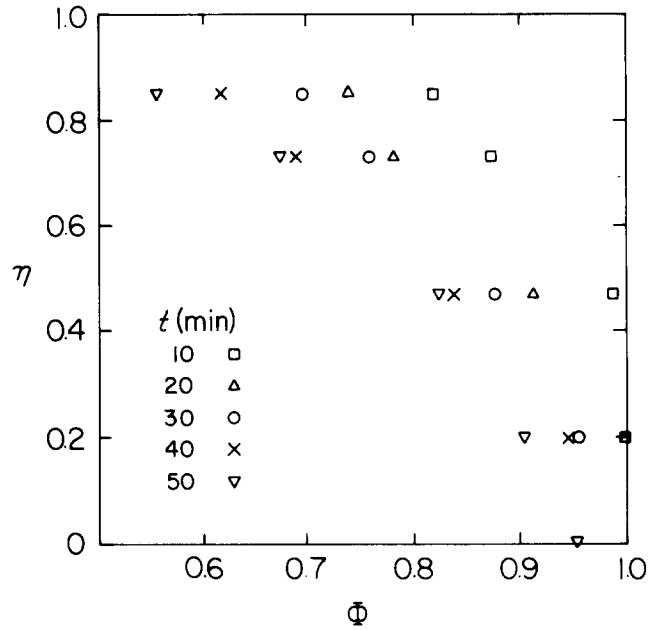
Figure 6. Concentration profiles for experiment M1.

compositional changes at the solid–liquid interface, while both the left and right walls are kept at the same temperature (ie, 0°C). The temperature measurements also indicate that the solid–liquid interface is not completely isothermal.

The shadowgraph images (Figs. 3a, 4a, and 5a) show that the stratified top layer is separated by a sharp ("double-diffusive") interface from the uncontaminated bottom layer. The development of such sharp interfaces is well known for heating (or cooling) a stable concentration gradient from the side [3]. It depends explicitly on the different diffusivities for heat and mass and is caused by the thermal natural convection flow in the bottom layer. Because the liquid effectively retains its (original) composition, the flow is constrained by the concentration (density) stratification and a definite interface is formed above the convecting layer. As mentioned above, the thermal buoyancy forces in experiment M1 are not strong enough to establish such convective layers in the stratified region in the upper part of the enclosure. Note that the double-diffusive interface is slightly tilted downwards away from the left wall. This can be attributed to the horizontal temperature drop between the left wall and the interface, which results in an increase in the density of the stratified fluid toward the interface. In addition, the convective flow along the left wall in the bottom layer effectively "pushes" the double-diffusive interface toward the top.

As shown in Figs. 3–5, the vertical extent of the stratified top layer increases continuously with time at the expense of the uncontaminated fluid region. The fluid flow and heat transfer patterns remain qualitatively the same as described above. At t = 30 min, almost the entire liquid is compositionally stratified. Figure 6 shows that the concentration near the top of the test cell continues to decrease, while the concentration gradient across the height of the enclosure becomes steeper. Note that at 50 min the liquid of the very bottom of the test cell is slightly diluted by the melt water (ie, $\Phi \approx 0.96$ at $\eta \approx 0$). Due to the decreasing height of the uncontaminated layer, thermal natural convection in this layer becomes weaker with

increasing time, while the dye becomes more concentrated (see Fig. 5b).

It can be seen that the double-diffusive convection patterns in the liquid have a profound influence on the local melting rates. Due to the presence of a thermal boundary layer along the interface in the uncontaminated bottom layer, the temperature gradients are large in this region (see Figs. 3b, 4c, and 5c). On the other hand, the temperature gradients at the interface in the stratified top layer are relatively small. Consequently, the interface moves faster in the bottom layer than in the stratified region. Since the extent of the stratified region continuously increases, the effects of a higher melting rate in the bottom convection layer are smeared out. After some time, the solid–liquid interface becomes curved, with the horizontal extent of the liquid region smoothly increasing from the top. The above discussion, however, does not explain the curvature of the interface *within* the uncontaminated layer, close to the bottom of the enclosure (see Figs. 3–5). This region is characterized by the development of the concentration boundary layer along the interface in which the flow is upward. Its thickness increases from zero at $\eta = 0$ to its maximum value at the top of the bottom convecting layer. Accordingly, the concentration gradients normal to the interface sharply increase toward $\eta = 0$. This results in a simultaneous increase in the local melting rate with decreasing η. No photographs are shown for times after 30 min, but they are available elsewhere [6]. It was observed, however, that at later times the melting rates continued to be very high at the bottom of the enclosure, while very little melting occurred over the remaining parts of the interface. After a long time (2 h), the ice at the bottom third of the enclosure was completely melted, leaving a small ice layer at the upper part of the right wall. As expected, the system reaches a steady state (after approximately 5 h), which is characterized by an isothermal (at 0°C) and quiescent liquid having a uniform composition, $\Phi = 0.5$. The later stages of the melting experiment are further discussed in connection with experiment M2.

Experiment M2. The shadowgraph images together with measured concentrations for experiment M2 are presented in Figs. 7. In experiment M2, the left wall temperature is considerably higher than in experiment M1, (ie, 40°C), and the right wall is below the eutectic temperature (ie, -20°C). While most of the transport and melting processes are similar to the ones described for experiment M1, there are some important differences that will highlight the complicated phenomena possible during melting with double-diffusive convection. As in experiment M1, liquid diluted by the melt water and confined in a thin concentration boundary layer rises along the solid–liquid interface and accumulates at the top of the enclosure. After some time, this results in a density stratification in the upper part of the liquid region, which is separated by a sharp, double-diffusive interface from the strongly convecting, uncontaminated liquid in the lower part of the enclosure. At approximately $t = 5$ min (see Fig. 7a), however, four double-diffusive interfaces appear above the original one, so that the liquid region now consists of five distinct layers of different concentrations. This indicates that inside the stratified region, natural convection takes place, which is driven by thermal buoyancy forces. In experiment M2, the thermal buoyancy forces are much stronger than in experiment M1 because of the larger temperature difference between the left wall and the solid–liquid interface (more than

40°C) and are therefore able to break up the stable stratification due to concentration. The liquid is heated by the left wall and rises through the stratified region. Since it retains its original composition, the heated liquid can rise only until it reaches a level where its density is equal to the density of the surrounding liquid in the concentration stratification. At that level, the flow turns horizontal toward the solid–liquid interface, where it is cooled again. Eventually, a clockwise rotating convection cell is established in the stratified region, which is bounded at the top by a double-diffusive interface. Due to the mixing by the flow, the liquid within each layer has a relatively uniform concentration. The development of such distinct layers in an initially smoothly stratified fluid is well known for side wall heating and cooling and has been studied in other contexts [3]. Similar observations have also been made by Huppert and Turner [4] for the melting of ice blocks into an artificially created salinity gradient.

As the melting progresses, the layers continue to grow (see Fig. 7b). After $t = 30$ min (Fig. 7b), most of the ice has melted, and the size of the layers, as well as their concentrations, changes relatively little (compare Figs. 7b and 7c). Interestingly, at approximately $t = 90$ min (Fig. 7d), the double-diffusive interface between the upper two layers breaks up and the liquid in the two layers mixes. The breakup of the interface is due to several factors. Because very little melting takes place after $t = 60$ min, the concentrations in the upper two layers become increasingly equal (see Fig. 7c). With a relatively small concentration difference across the double-diffusive interface, the thermal buoyancy forces become dominant over the solutal forces. Since the thermal natural convection flow is upwards at the left (hot) wall, the interface adjacent to this wall is "pressed" toward the top of the enclosure. The opposite is true for the double-diffusive interface adjacent to the solid. Eventually, the thermal natural convection flow penetrates the double-diffusive interface, resulting in the mixing of the liquid in the two layers (see Fig. 7d). At $t = 105$ min, the liquid region consists of three well-mixed layers [6]. The concentrations in the lower two layers are approximately equal to the ones at $t = 60$ min, while the concentration in the upper layer represents an average of the concentrations measured in the upper two layers present at $t = 60$ min [6]. This merging process of the upper two layers is repeated at approximately $t = 110$ min [6], so that the liquid region at $t = 120$ min (Fig. 7e) consists of only two layers. After a long time (about 180 min), experiment M2 reaches a steady state characterized by a single convection cell in the liquid ($\Phi \approx 0.55$) and a thin ice layer at the right wall.

The larger thermal buoyancy forces in experiment M2 also cause the convection cells within each double-diffusive layer to be stronger. This is reflected by the shape of the solid–liquid interface, which is particularly evident in the lower layer at $t = 5$ and 30 min (Figs. 7a and 7b, respectively). Because the temperature of the liquid decreases as it flows downwards along the solid–liquid interface, the melting rate decreases toward the bottom of each layer. After some time, this results is a curved solid–liquid interface within each layer, with the horizontal extent of the solid increasing toward the bottom. In fact, a close examination of Figs. 7 reveals that there are "step" changes in the thickness of the ice at the vertical locations where the double-diffusive interfaces are present. Since the liquid flows in a different direction on each side, the solid–liquid interface is quite pointed at the right end of each double-diffusive interface. Such complex solid–liquid interface

Φ =0.361—
0.631—
0.927—

(a)

0.448—
0.587—
0.675—
0.775—

(b)

0.296—
0.370—
0.527—
0.666—

(c)

(d)

0.462—
0.631—

(e)
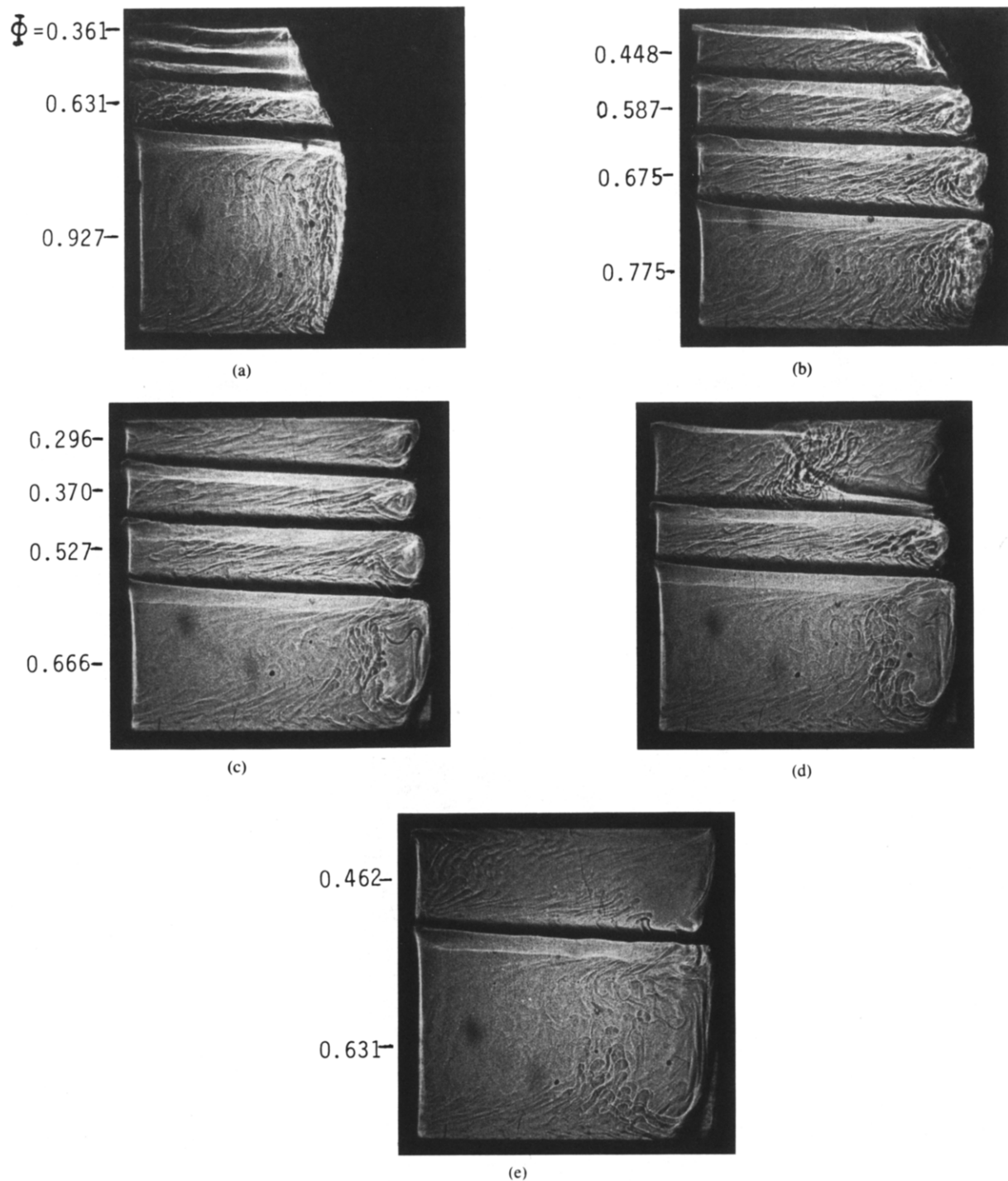
Figure 7. Shadowgraphs and concentrations for experiment M2.
(a) $t = 5$ min; (b) $t = 30$ min; (c) $t = 60$ min; (d) $6 = 90$ min;
(e) $t = 120$ min.

shapes have also been observed in studies of free convection melting of ice in saline water [8–11]. Due to the changing size of the layers, the locations of the steps in the solid–liquid interface move continuously. For example, a comparison of Figs. 7c, 7d, and 7e shows that, owing to the merging of the layers, the steps present in the ice at earlier times (eg, $t = 60$ min) have melted, and new steps have formed at the right end of the double-diffusive interfaces at later times (eg, $t = 90$ or 120 min). This resolidification is possible in experiment M2 because the right wall is below the eutectic temperature (ie, $T_2 = -20°C$). Accordingly, complete melting of the solid does not occur, and the double-diffusive processes in the liquid can indeed induce resolidification during the later stages of the experiment.

(a)

(b)

(c)

$\Phi = 0.078-$

$0.178-$

$0.797-$

(d)

(e)
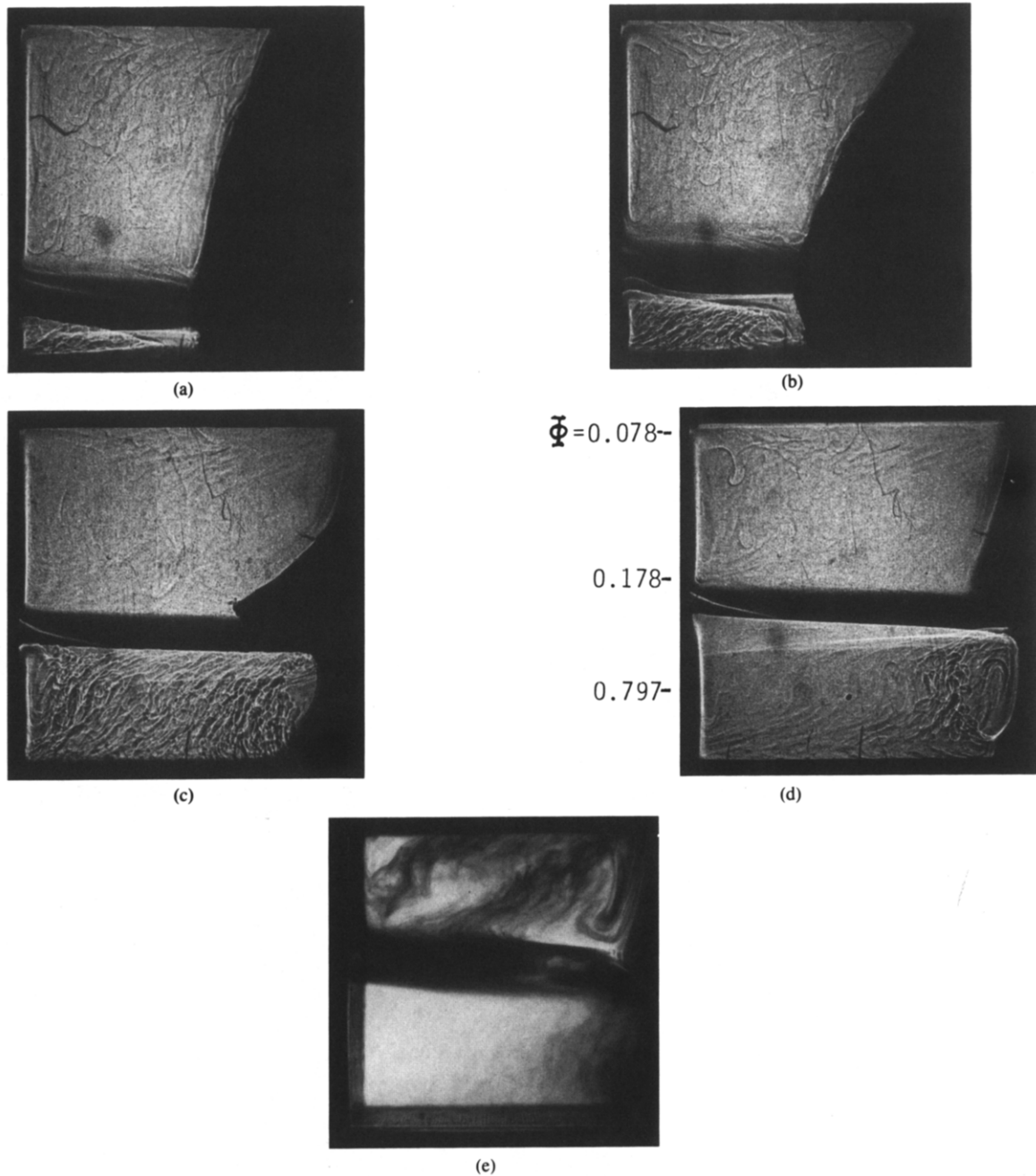
Figure 8. Shadowgraphs, flow visualization, and concentrations
for experiment M3. (a) $t = 2$ min; (b) $t = 5$ min; (c) $t = 15$ min;
(d) $= 60$ min; (e) $t = 70$ min.

Melting of an Ammonium Chloride–Water Eutectic into Water: Experiment M3

Experiment M3 (Fig. 8) is, in many respects, opposite to the previously discussed melting experiments. When the NH$_4$Cl–H$_2$O eutectic melts, the water adjacent to the solid–liquid interface becomes rich in NH$_4$Cl. This concentration change causes the density of the liquid to increase. A further density increase is caused by the cooling of the solid–liquid interface. Hence, the cold and contaminated water flows downwards along the solid–liquid interface in a boundary layer. As opposed to experiments M1 and M2, the thermal and solutal buoyancy forces in this boundary layer augment each other. At the bottom of the cavity, the cold and contaminated liquid accumulates in a layer of higher NH$_4$Cl concentration. As indicated by the concentration measurements, the water in the upper region of the test cell, outside of the concentration boundary layer, remains relatively uncontaminated. Thermal buoyancy forces establish convection cells in the NH$_4$Cl-rich layer at the bottom as well as in the relatively uncontaminated

upper layer (see Fig. 8e). Consequently, a sharp, double-diffusive interface is formed between the two liquid layers. Due to the mixing by the convective flow, both the upper and lower layers have a relatively uniform concentration (see Fig. 8d). As melting progresses, the NH_4Cl-rich bottom layer continues to grow so that the double-diffusive interface moves slowly upwards.

The double-diffusive phenomena described above have a profound influence on the melting process. Unlike experiments M1 and M2, the melting rate is higher toward the top of the enclosure, so that the horizontal extent of the solid increases smoothly toward the bottom. This can be attributed to the developing concentration boundary layer along the solid–liquid interface. The thickness of this boundary layer is zero at the top of the enclosure, increases toward the bottom, and reaches a maximum at the vertical location where the double-diffusive interface is present. Consequently, the concentration gradient in the liquid normal to the solid–liquid interface, and hence the melting rate, decreases from the top toward the double-diffusive interface. Interestingly, there exists at all times a step change in the thickness of the solid at the vertical location of the double-diffusive interface. At this location, the solid–liquid interface is almost horizontal. On the other hand, in the bottom layer the solid–liquid interface becomes vertical again. This step in the solid thickness results in a relatively large horizontal extent of the bottom layer compared to the upper layer above the double-diffusive interface. The reasons for the step change in the thickness of the solid are the following. Since the right wall is maintained below the eutectic temperature ($T_2 = -20°C$), the temperature of the solid–liquid interface can be expected to be relatively low. In fact, for a small solid thickness the interface temperature is below the liquidus temperature of the almost uncontaminated water in the upper layer. At later times, this causes water to solidify on the remaining NH_4Cl–H_2O eutectic in the upper layer. The formation of a (transparent) ice layer in the upper portion of the enclosure can clearly be seen in the flow visualization picture (Fig. 8e). The ice cover inhibits further melting of the NH_4Cl–H_2O eutectic, so the solid–liquid interface adjacent to the upper layer becomes stationary. Due to the higher NH_4Cl concentration, the liquidus temperature of the liquid in the bottom layer, however, remains below the solid–liquid interface temperature. Hence, there is no ice formed in the lower layer, and the NH_4Cl–H_2O eutectic continues to melt. Complete melting of the solid does not take place, because the right wall is below the eutectic temperature. After approximately $t = 60$ min, the phase-change processes, as well as the upward movement of the double-diffusive interface, become very slow. At steady state, however, the liquid is expected to be at a uniform concentration. Hence, the double-diffusive interface and the step change in the solid thickness are not expected to exist at steady state [6].

CONCLUSIONS

An experimental study has been performed of the melting of a vertical ice layer into an NH_4Cl–H_2O solution, as well as that of a vertical NH_4Cl–H_2O eutectic layer into water. The experiments were conducted inside a vertical rectangular cavity with differentially heated side walls. In both cases, it is found that the melting process induces the formation of double-diffusive layers in the initially homogeneous liquid. The experiments indicate that relatively small changes in the

thermal boundary conditions can result in considerable differences in the layering process. Due to the continuously changing concentrations in each layer, the double-diffusive interfaces can break up, resulting in vigorous mixing of the liquid in the layers.

It is conclusively shown that the double-diffusive phenomena in the liquid also have a significant influence on the melting processes. This is reflected by strong variations in the local melting rates over the height of the solid layer. For example, the presence of double-diffusive interfaces in the liquid causes the formation of steps in the solid layer thickness. In cases where the side wall bounding the solid layer is held below the eutectic temperature, it is found that the convection phenomena can even induce resolidification on parts of the remaining solid layer.

NOMENCLATURE

C concentration, kg/kg
H height of enclosure, m
L length of enclosure, m
s liquid layer thickness, $(= S/L)$, dimensionless
S liquid layer thickness, m
t time, s
T temperature, K
x horizontal coordinate, m
y vertical coordinate, m

Greek Symbols

Γ slope of liquidus line, K
η vertical coordinate $(= y/L)$, dimensionless
θ temperature $[= (T - T_E)/(T_1 - T_E)]$, dimensionless
κ segregation coefficient $(= C_{s,i}/C_{l,i})$, dimensionless
ξ horizontal coordinate $(= x/L)$, dimensionless
Φ concentration $(= C/C_E)$, dimensionless

Subscripts

E eutectic
i interface
in initial
l liquid
p pure
s solid
1 left side (liquid)
2 right side (solid)

REFERENCES

1. Fisher, K. M., The Effects of Fluid Flow on the Solidification of Industrial Castings and Ingots, *PhysicoChem. Hydrodyn.*, **2**, 311–326, 1981.
2. Pimputkar, S. M. and Ostrach, S., Convective Effects in Crystal Growth from Melt, *J. Crystal Growth*, **55**, 614–646, 1981.
3. Turner, J. S., and Gustafson, L. B., Fluid Motions and Compositional Gradients Produced by Crystallization or Melting at Vertical Boundaries, *J. Volcanol. Geotherm. Res.*, **11**, 93–125, 1981.
4. Huppert, H. E., and Turner, J. S., Ice Blocks Melting into a Salinity Gradient, *J. Fluid Mech.*, **100**, 367–384, 1980.

5. Chen, C. F., and Johnson, D. H., Double-Diffusive Convection: A Report on an Engineering Foundation Conference, *J. Fluid Mech.*, **138**, 405–416, 1984.

6. Beckermann, C., Melting and Solidification in Binary Systems with Double-Diffusive Convection in the Melt, Ph.D. Thesis, Purdue University, West Lafayette, Ind., 1987.

7. Beckermann, C., and Viskanta, R., Double-Diffusive Convection Due to Melting, *Int. J. Heat Mass Transfer*, (in press), 1988.

8. Carey, V. P., and Gebhart, B., Transport Near a Vertical Ice Surface Melting in Saline Water: Experiments at Low Salinities, *J. Fluid Mech.*, **117**, 403–423, 1982.

9. Sammakia, B., and Gebhart, B., Transport Adjacent to Ice Surfaces Melting in Saline Water: Visualization Experiments, *Int. Commun. Heat Mass Transfer*, **11**, 25–34, 1984.

10. Johnson, R. S., and Mollendorf, J. C., Transport from a Vertical Ice Surface Melting in Saline Water, *Int. J. Heat Mass Transfer*, **27**, 1928–1932, 1984.

11. Josberger, E. G., and Martin, S., A Laboratory and Theoretical Study of the Boundary Layer Adjacent to a Vertical Melting Ice Wall in Salt Water, *J. Fluid Mech.*, **111**, 439–473, 1981.

12. Beckermann, C., and Viskanta, R., Double-Diffusive Convective during Dendritic Solidification of a Binary Mixture, *PhysicoChem. Hydrodyn.*, **10**, 195–213, 1988.

13. Beckermann, C., and Viskanta, R., An Experimental Study of Solidification of Binary Mixtures with Double-Diffusive Convection in the Liquid, in *ASME Proceedings of the 1988 National Heat Transfer Conference*, H. R. Jacobs, Ed., HTD-96, Vol. 3, pp. 67–79, ASME, New York, 1988.

14. *International Critical Tables of Numerical Data, Physics, Chemistry and Technology*, Vol. 3, p. 60, and Vol. 4, p. 218, 1928.